ELSEVIER

Journal of Photochemistry and Photobiology A: Chemistry 118 (1998) 25–30

Journal of Photochemistry and Photobiology A:Chemistry

Effects of oxygen and temperature on phosphorescence and delayed fluorescence of erythrosin B trapped in sol–gel silica

Sio Kuan Lam, Ebinazar Namdas, Dennis Lo*

Department of Physics, The Chinese University of Hong Kong, Shatin, NT, Hong Kong, China

Received 24 February 1998; received in revised form 2 June 1998; accepted 15 July 1998

Abstract

Room temperature phosphorescence (RTP) of erythrosin B in sol–gel silica was studied in ambient air, in pure oxygen and in vacuum. Oxygen was found to be an effective quencher of RTP. The phosphorescence and delayed fluorescence data at oxygen pressures higher than 20 mbar can be interpreted by Stern–Volmer diffusional theory. The quenching rate constants of oxygen were determined to be 0.0151 and 0.0111 $mbar^{-1}$, respectively for phosphorescence and delayed fluorescence. Phosphorescence spectrum at 97°K was measured. More than 2-folds enhancement of phosphorescence intensity was achieved at 97°K. The phosphorescence quantum yields in vacuum were determined as 5.0% and 2.0% at 97°K and at room temperature, respectively. © 1998 Elsevier Science S.A. All rights reserved.

Keywords: Phosphorescence; Erythrosin B; Sol–gel; Oxygen; Temperature

1. Introduction

Organic dyes in the solid matrices have been the subject of considerable research interest because of its potential use in a wide range of applications (e.g. laser devices [1–5], optical nonlinearity [6–10], optical sensors [11–13], etc.) Dyes trapped in solid cage possess large third-order susceptibilities because of the long decay lifetimes of the lowest triplet state, making possible applications as optical limiters, or optical logic switch [6,9]. Study of the phosphorescence spectroscopy should shed lights on the triplet state dynamics and thus the third-order nonlinear susceptibility of dye-doped solids. Most of the work on dye-doped solids was done in boric acid glass and polymeric materials such as PMMA, PVA, gelatin, etc. These host materials transmit poorly in the UV, and have poor processibility. They also tend to degrade mechanically and optically after prolonged use. Sol–gel-derived silica shows good promise as host for organic dyes molecules [14]. It enjoys superior thermal and optical properties and possibly better processibility than boric acid glass, PMMA and gelatin. We have been studying dye-doped sol–gel-derived silica as solid state laser materials and as nonlinear optical devices [2,3,16].

Oxygen is a very effective quencher for the luminescence process of dye molecules in liquid solvents and in some solid matrices [4,5,15]. The role of oxygen is, therefore, critical but detrimental to the performance of devices based on dye-doped solids. Very recently, while working on solid state dye lasers, Rahn et al. [5] found that the oxygen is the main factor in the photodestruction process of dyes in modified (polymethyl methacrylate) (MPMMA) and in polycom glass. Faloss et al. [15] fabricated deoxygenated pyrromethene 597-doped ormosil glass and demonstrated improvements by a factor of 10 in photostability. Although there is no doubt as to the detrimental role of oxygen in dye-doped solid devices, there has been few detailed report on the influences of oxygen in dye-doped sol–gel silica.

In a previous paper we reported on the time resolved spectroscopic study of xanthene dyes in wet silica gel [15]. The dye erythrosin B was chosen because it was known to have high triplet state yield, long triplet state lifetime and hence large third-order nonlinear susceptibility in gelatin [28]. Our study aimed to reveal if sol–gel silica matrix holds promise as a host for erythrosin B for nonlinear optics applications. To follow up our previous work, we report here our recent spectroscopic results on the effects of oxygen and temperature on phosphorescence and delayed fluorescence of erythrosin B in dry sol–gel silica. Strong quenching of the phosphorescence by oxygen was demonstrated. The quenching behavior was discussed by considering the Stern–Volmer-type diffusional effect. The emission spectra at 97°K were also studied. Quantum yields of fluorescence, phosphorescence and delayed fluorescence of erythrosin B in

*Corresponding author. Tel.: +852-2609-6103; fax: +852-2603-5204; e-mail: dlo@phy.cuhk.edu.hk

1010-6030/98/$ – see front matter © 1998 Elsevier Science S.A. All rights reserved.
PII: S1010-6030(98)00350-5

sol–gel silica were measured in air, in pure oxygen and in vacuum at room temperature and at 97°K. The phosphorescence peak is 5 nm blue shifted as compared to that at room temperature.

2. Experimental

The following chemicals were used in the sol–gel sample preparation: tetramethoxysilane (TMOS, ACROS, 99% grade), methanol, sodium hydroxide, erythrosin B (Aldrich). They were used as received without further purification.

2.1. Dye-doped sol–gel silica

The dye-doped sol–gel silica in bulk form was prepared according to the sol–gel process of base catalyzed hydrolysis. TMOS (10 ml), methanol (12 ml), deionized water (7.4 ml) and 0.1 M NaOH (1.6 ml) were mixed under magnetic stirring at room temperature. Dye was added to the mixture and the resulting solution (sol) was casted in acrylic cuvettes that were then sealed with sticky tapes. The sol gelled within 10 min at room temperature. The seals were removed after 3 days. The gels were allowed to dry, shrink and age further in the ambience at room temperature. After 2 weeks the gels were baked at 115°C for 10 h. The sol–gel samples, thus, prepared were relatively dry and free of residual reactants. These bulk dye-doped sol–gel samples typically measured at 6 mm (w) × 6 mm (h) × 12 mm (l). The concentration of the erythrosin B in starting solution was 2.3×10^{-4} mol l^{-1}. Note that in our previous work on time-resolved phosphorescence spectroscopy of erythrosin B-doped sol–gel silica [15], the baking process at 115°C was omitted. The resulting gels were, therefore, considered wet.

2.2. Luminescence measurements

A sketch of our experimental set-up is shown in Fig. 1. The stainless steel test chamber was fitted with inlet port and evacuation port for gas fills and evacuation purposes. Light signals were monitored through several view ports fitted with optical flats. The sample holding platform was part of a cold finger that can be liquid-nitrogen cooled to 97°K as determined by a thermo-couple. The entire test chamber was vacuum tested to be leak-free and to maintain a vacuum level better than 0 mbar (as indicated by the analog pressure gauge). All samples were degassed in vacuum for 1 day before measurements.

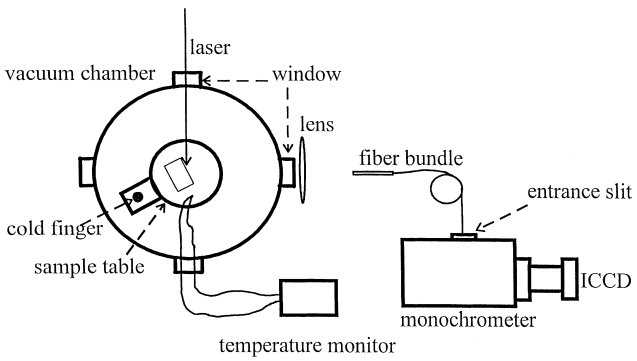

Fig. 1. Schematic diagram of luminescence experimental set-up.

Luminescence of the samples was induced by 5 ns (FWHM) pulses of the second harmonic of a Nd:YAG laser (Continuum, Surelite II). Luminescence from the sample 90° to the direction of Nd:YAG laser beam was imaged onto a fiber bundle mounted in close proximity to the samples. The other end of the fiber bundle was connected to the entrance slit of a 0.3 m grating monochrometer (SpectraPro 300I, ARC) configured as a spectrograph in the present work. A gatable intensified charge couple device (TE-ICCD Princeton Instrument) was mounted on the output focal plane of the monochrometer to detect and analyze the emission spectra.

The timing sequence in the detection of an emission spectrum was described in our previous paper [16]. In our experiments, the time-integrated fluorescence spectra was collected by setting the delay time (the time between the onset of the laser pulse and the onset of the gate pulse) to zero and the gate width (exposure time of the ICCD) to 70 ns. The 70 ns gate width was chosen as it is much longer than the fluorescence decay (a few ns) but very short compared to the decay times of both RTP and DF so that the influence of delayed luminescence could be minimized. When the delayed luminescence (phosphorescence plus delayed fluorescence) spectra were collected, the delay time was set at 70 ns to screen off the fluorescence signals. Also, the gate width was set to 80 ms to allow time-integration of the entire phosphorescence and delayed fluorescence signals. All spectra presented had been corrected for the combined spectral sensitivity of the ICCD, monochrometer and fiber bundle.

The luminescence quantum yields (i.e., fluorescence, phosphorescence and delayed fluorescence) were measured by using front surface excitation emission geometry [16–19]. Rhodamine 6G (R6G) in methanol was used as reference with a fluorescence quantum yield of 0.96 for calculation of quantum yield data. The area under the curve of emission spectra was used for calculation of quantum yield. Refractive index corrections for the sol–gel samples as well as for R6G in methanol were applied.

3. Results and discussions

3.1. Room temperature luminescence

Emission spectra of erythrosin B (Its molecular structure is well-known and given in our previous work [16].) were first measured in ambient air and in vacuum. Table 1 shows

Table 1
Spectroscopic parameters of erythrosin B in various solid matrices and temperatures

	λ_f (nm)[a]	λ_p (nm) [a]	Φ_f (%)[b]	Φ_{df} (%)[b]	Φ_p (%)[b]
Sol–gel in air ambience, room temperature	565.4	—	1.7	~0.0047	~0.014
Sol–gel in vacuum, room temperature	565.4	702.3	2.0	0.085	2.1
Sol–gel in vacuum, 97°K	567.6	697 .9	3.3	0	5.0
Gelatin in air ambience. room temperature	562.6	—	2.1	—	—
H_2O	534	—	2.0	—	—

[a]Uncertainty in wavelength data is ±1 nm.
[b]Uncertainty in quantum yield is ±10%.

the measured spectroscopic parameters of erythrosin B in sol–gel silica. The parameters include wavelength of fluorescence maxima, phosphorescence maxima, fluorescence quantum yield, phosphorescence quantum yield and delayed fluorescence quantum yield. For comparison, the respective parameters of erythrosin B in gelatin and in water are also listed in Table 1. The fluorescence quantum yield was measured to be 2.0% and 1.7% for samples in vacuum and in ambient air, respectively. These values are in good agreement with the reported value (2.0%) in the literature [20]. The differences of fluorescence quantum yields in ambient air and in vacuum were small and believed to be within the margin of experimental error. Further evidence will be provided in Table 2.

From Table 1, the fluorescence and phosphorescence peaks were found to be 565.4 and 702.3 nm, respectively. There is a slight red shift of 2–3 nm of the peaks of the fluorescence and phosphoresce spectra of the sol–gel samples as compared to those in gelatin. The red shift in sol–gel silica can be attributed to the solvatochromic and local environmental effects of the silica matrix [21].

All sol–gel samples show very weak and barely detectable phosphorescence in air ambience. Intense phosphorescence was, however, observed in vacuum. Fig. 2 shows typical fluorescence and delayed luminescence spectra of erythrosin B in sol–gel silica in vacuum at room temperature. The quantum yields were determined as 2.1% and 0.085%, respectively for phosphorescence and delayed fluorescence in vacuum at room temperature. We attribute the enhancement of phosphorescence in vacuum to the removal of oxygen from the silica cage. Because of the porosity of the silica gel, oxygen in the air is believed to easily diffuse into the sol–gel silica matrix when exposed to open air. Consequently, triplet state dye molecules are effectively quenched by oxygen and very little phosphorescence can be detected.

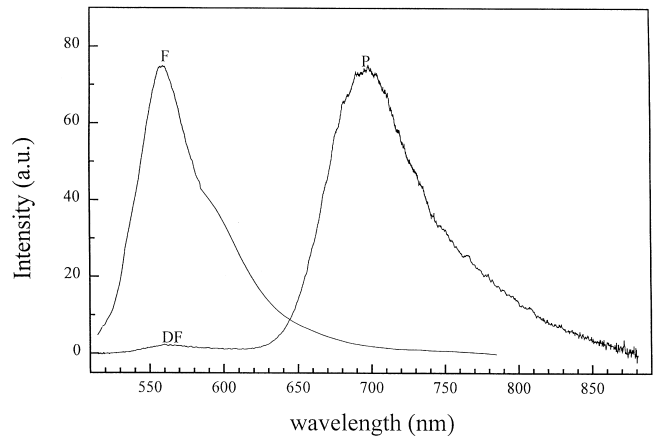

Fig. 2. Fluorescence and delayed luminescence spectra of erythrosin B in sol–gel silica at room temparature and in vaccum. F, DF and P denote fluorescence, delayed fluorescence and phosphorescence, respectively.

Table 2
Quantum yields of fluorescence, delayed fluorescence and phosphorescence of erythrosin-doped sol–gel silica at various oxygen pressures

Oxygen pressure (mbar)	Φ_f (%)	Φ_{df} (%)	Φ_p (%)
0	2.0	0.097	2.0
20	2.1	0.073	0.17
40	2.0	0.045	0.11
100	2.1	0.034	0.082
200	2.1	0.016	0.49
500	2.1	0.006	0.027
800	2.0	0.005	0.016
1000	2.0	0.004	0.014

To ascertain the role of oxygen, we carried out a systematic study on the phosphorescence quenching by varying the oxygen pressure. Delayed luminescence spectra (at delay time of 70 ns) were measured by keeping the samples in pure oxygen environment. The oxygen pressure was varied from 0 to 1000 mbar. Fig. 3 shows the delayed emission spectra recorded at various ambient oxygen pressure. Curves numbered from 1 to 6 represent the spectra recorded at oxygen pressure of 0, 20, 40, 100, 200, and 500 mbar, respectively. It is obvious that the intensity of delayed luminescence, especially phosphorescence, decreases as oxygen pressure increases. By comparing the integrated area under phosphorescence peak and delayed fluorescence peak at various pressures, the respective quantum yields were determined. The data were plotted in Fig. 4 and listed in Table 2. Clearly, as pressure/concentration of oxygen increases the quantum yield decreases.

The oxygen quenching process can be described by the Stern–Volmer equations as [22]

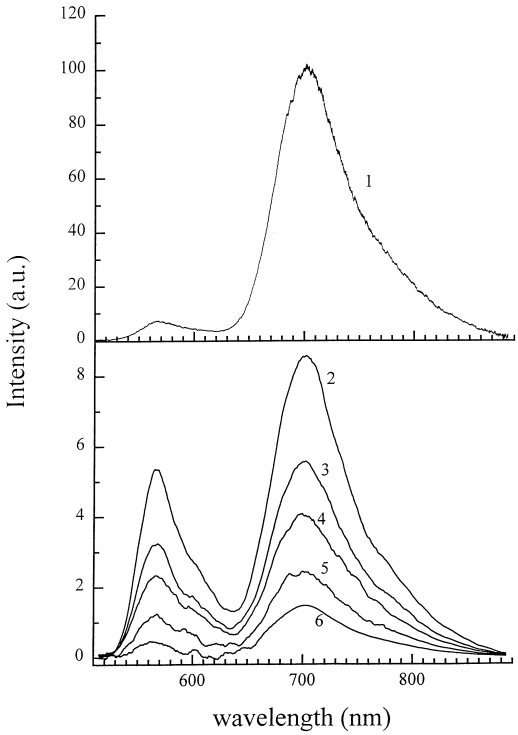

Fig. 3. Delayed luminescence at oxygen pressures of 0 mbar (1), 20 mbar (2), 40 mbar (3), 100 mbar (4), 200 mbar (5), and 500 mbar (6) for curves (1)–(6), respectively.

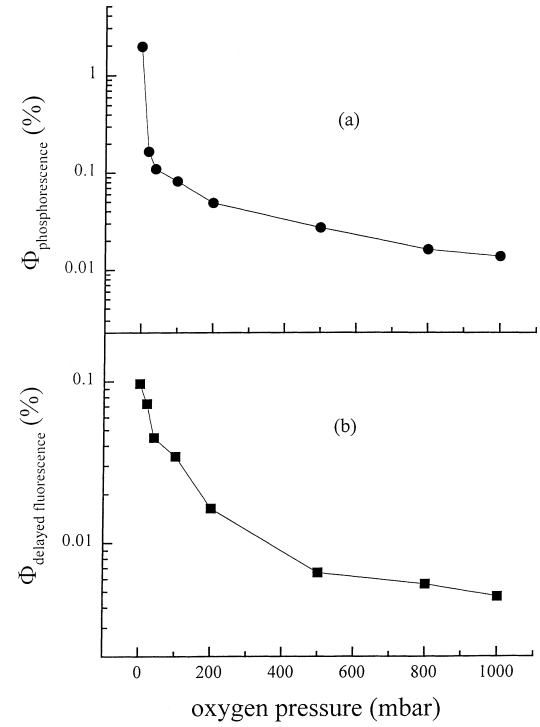

Fig. 4. Quantum yields of phosphorescence (a) and delayed fluorescence (b) as a function of oxygen pressure.

$$\frac{\Phi_0}{\Phi} = 1 + K_{sv}[O_2] \quad (1)$$

$$K_{sv} = k\tau_0 \quad (2)$$

$$k = \alpha D \quad (3)$$

where Φ is luminescence quantum yield, Φ_0 and τ_0 are luminescence quantum yield and the excited state lifetime of the fluorophore in the absence of quencher, respectively. K_{sv} is the Stern–Volmer quenching rate constant. k is the diffusion-dependent bimolecular quenching constant. α is the oxygen solubility coefficient in the environment of fluorophore. The solubility coefficient and diffusion coefficient, D determine the bimolecular quenching constant k for a given fluorophore.

Fig. 5 shows the plot of Φ_0/Φ vs. ambient oxygen pressure. We take the value of Φ at 20 mbar as Φ_0 for reasons that we will explain in the next paragraph. Both ratios of phosphorescence and delayed fluorescence can be very well

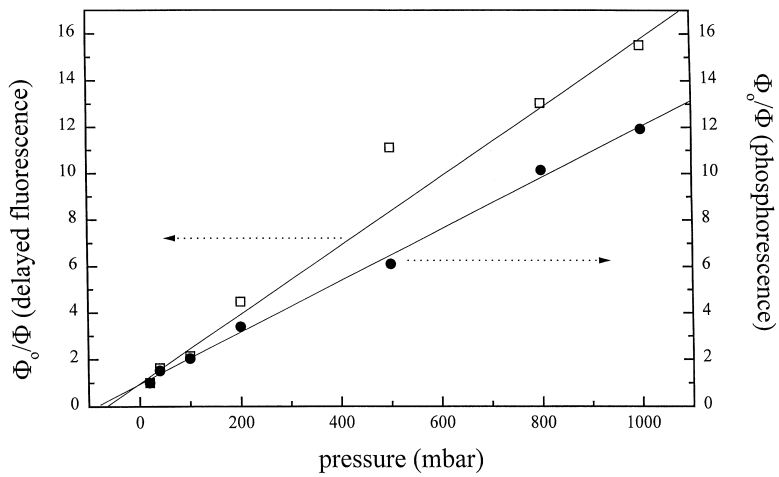

Fig. 5. The ratio of Φ_0/Φ of phosphorescence and delayed fluorescence versus oxygen pressure.

fitted by Stern–Volmer equation. The quenching rate constants (K_{sv}) were found to be 0.0151 and 0.0111 mbar^{-1} for delayed fluorescence and phosphorescence, respectively. The two K_{sv} values were almost identical within the margin of experimental error. This is so because delayed fluorescence originates from the triplet state via thermal activation [16] and hence should have the same lifetime as phosphorescence. Since oxygen effectively quenches the triplet state, the two quenching rate constants should be the same [16,23].

Similar quenching rate constants cannot be deduced from data taken at less than 20 mbar. One would note in Fig. 4 that at around 0 mbar (actually $\sim 10^{-4}$ bar in our estimation) the phosphorescence decrease much more rapidly than the delayed fluorescence. In Table 2, it is clear that the Φ_p decreases from 2.0% at 0 mbar to 0.17% at 20 mbar while delayed fluorescence decreases from 0.097% to 0.073% for the same variation in pressure, indicating different quenching rate constants for the two processes. The difference cannot be attributed to the signal fluctuation in our experiments as the phosphorescence has the strongest intensity at 0 mbar. The quenching dynamics of oxygen seems to be different at high (>20 mbar) and low (<20 mbar) pressures. Also, we cannot rule out the possibility of quenching by impurity species at low pressures ($\sim 10^{-4}$ bar) in our experiments. We are, however, unable to study the quenching process below 20 mbar in more detail due to the resolution limitation of the analog pressure gauge used in these experiments (it has a minimum scale of 20 mbar). Clarification of the quenching process of phosphorescence at such low pressure ($\sim 10^{-4}$ bar) await further study.

From Table 2 we also note that the oxygen quenching is not very effective for fluorescence. This is so because the singlet state lifetime is short compared to the quenching reaction time by oxygen.

3.2. Low temperature luminescence

Sol–gel samples were cooled to 97°K by pouring liquid nitrogen into the dewar of the cold finger set-up. Fluorescence, delayed fluorescence and phosphoresce of erythrosin B sol–gel samples at 97°K were measured. Fig. 6(a) shows the fluorescence spectra of erythrosin B in sol–gel silica at room temperature and at 97°K in vacuum. The respective spectroscopic data of erythrosin B at 97°K were listed in Table 1. The shape of the fluorescence spectra at room temperature and at 97°K is almost the same. The value of fluorescence quantum yield is doubled at 97°K. The enhancement of fluorescence quantum yield at liquid nitrogen temperature is a result of the decrease in the reaction rates of the temperature-dependent internal conversion processes (from the singlet upper state to the lowest triplet state).

Fig. 6(b) shows the delayed luminescence spectra of the sol–gel samples at 97°K and at room temperature. Clearly,

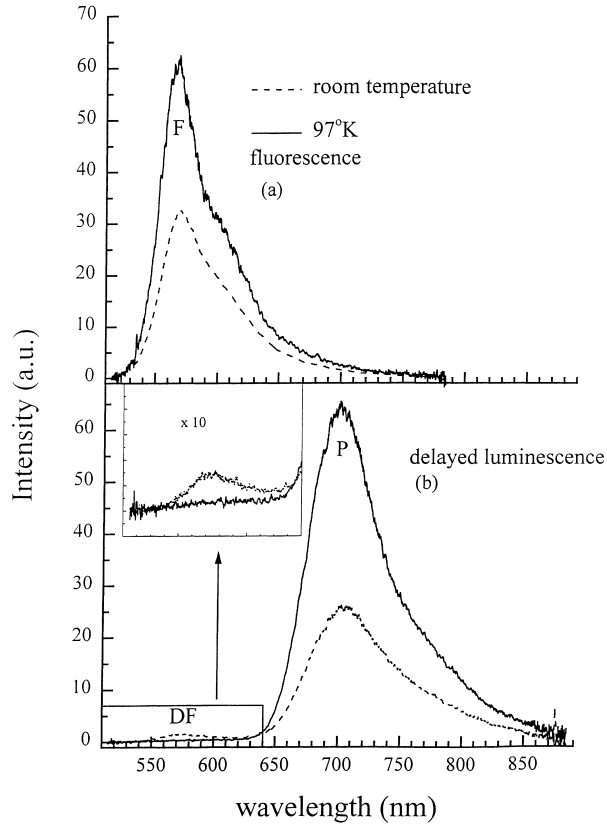

Fig. 6. (a) Fluorescence spectra of erythrosin B in sol–gel silica at 97°K. (b) Delayed luminescence spectra of erythrosin B in sol–gel silica at 97°K.

the delayed fluorescence peak disappears at 97°K. This indicates that the thermal activation mechanism from the lowest triplet state to the singlet upper state, the main population route of the delayed fluorescence, slows at low temperature. In addition, the phosphorescence intensity was enhanced as the quantum yield was measured to be 5.0% at 97°K. Comparing with the result at room temperature, the phosphorescence quantum yield increases by a factor of 2.5. At low temperature thermal relaxation from triplet to the ground state slows, and phosphorescence yield increases as a result.

We also observe that the peak of the phosphorescence spectrum at 97°K is blue-shifted by 5 nm as compared to that at room temperature. Similar blue shift of the peak of the phosphorescence spectra was observed for the case of butyrophenone at 77°K in 1 : 1 and 9 : 1 iso pentene–methylcyclohexence mixture [24]. The very viscous 1 : 1 iso pentene–methylcyclohexence mixture at 77°K gives high energy band as compared to 9 : 1, iso pentene–methylcyclohexence mixture, a less viscous solvent at 77°K. The observed blue shift was explained in terms of a microviscosity model [24]. More closely related to our work on dye-doped sol–gel silica, Casalboni et al. [25] recently reported on a spectroscopic study of the saturable absorber 3,3′-diethyloxadicarbocyanine iodide (DODCI) embedded in silica

sol–gel glass. Comparing with the results in methanol solution, a 20 nm blue shift was observed in dye-doped sol–gel silica for both the absorption and emission bands. Physical restriction on the molecular photoisomerization rearrangement caused by the rigidity of the silica cage was cited as the reason [25].

In our case, increase in microviscosity or physical restriction of the sol–gel samples at low temperature may be traced to the presence of water and organic residuals within the ultraporous sol–gel silica structure [26,27]. Although the sol–gel samples were baked at 115°C, organic and water residues remain trapped in the microenvironment. They freeze at 97°K and thus lead to an increase of the microviscosity or physical restriction of the sol–gel samples. The elimination of organic and water residues can only be completed by sintering the sol–gel samples at temperature higher than 850°C [27].

4. Conclusions

Oxygen quenching of RTP of erythrosin B was demonstrated. Stern–Volmer theory was applied to interpret the oxygen quenching effect. The quenching rates were determined to be 0.0151 and 0.0111 $mbar^{-1}$ for delayed fluorescence and phosphorescence, respectively. Emission spectra and quantum yields (fluorescence, delayed fluorescence and phosphorescence) of erythrosin B in sol–gel silica were measured under various conditions. Samples at 97°K in vacuum give the highest phosphorescence quantum yield of 5.0% while the quantum yield is almost zero at room temperature in air. The phosphorescence peak is 5 nm blue-shifted as compared to the room temperature phosphorescence peak.

Acknowledgements

This work is supported in part by a RGC Grant project no. 2150105.

References

[1] R. Reisfeld, D. Brusilovsky, M. Eyal, E. Miron, Z. Burstein, J. Irvi, Chem. Phys. Lett. 160 (1989) 43.
[2] D. Lo, J.E. Parris, J.L. Lawless, Appl. Phys. B 55 (1992) 363.
[3] C. Ye, K.S. Lam, S.K. Lam, D. Lo, App. Phys. B. 65 (1997) 109.
[4] A.V. Deshpande, E.B. Namdas, Chem. Phys. Lett. 263 (1996) 449.
[5] M.D. Rahn, T.A. King, A.A. Gorman, I. Hamblett, App. Opts. 36 (1997) 5862.
[6] D.S. Chemla, J. Zyss (Eds.), Non-linear Optical Properties of Organic molecules and Crystals, Academic Press, 1987, pp. 1–2.
[7] Y. Cui, B. Swedek, N. Cheng, K.S. Kim, P.N. Prasad, J. Phys. Chem. B. 101 (1997) 3530.
[8] T. Sugihara, K. Fujii, H. Haga, S. Yamamoto, App. Phys. Lett. 69 (1996) 2971.
[9] K.K. Sharma, K.D. Rao, G.R. Kumar, Opt. Qunatum Electron. 26 (1994) 1.
[10] C. Branger, M. Lequan, R.M. Lequan, M. Large, F. Kajzar, Chem. Phys. Lett. 272 (1997) 265.
[11] B.D. Gupta, D.K. Sharma, Opts. Comm. 140 (1997) 32.
[12] Y. Sadaoka, Y. Sakai, Yu. Uki, Talanta 39 (1992) 1675.
[13] G.J. Mohr, I. Murkovic, F. Lehmann, C. Haider, O.S. Wolfbeis, Sens. Actuators B. B3 (1997) 239.
[14] D. Avnir, D. Levy, R. Reisfeld, J. Phys. Chem. 88 (1984) 5956–5959.
[15] M. Faloss, M. Canva, P. Georges, A. Brun, F. Chaput, J.P. Boilot, Advanced solid state dye lasers, S.A. Payne, C.R. Pollock (Eds.), OSA Trends in Optics and Photonics Series, vol. 1, 1996, p. 69.
[16] S.K. Lam, D. Lo, Chem. Phys. Letts. 281 (1997) 35.
[17] J.N. Demas, G.A. Grosby, J. Phy. Chem. 75 (1971) 991.
[18] R.J. Hurtubise, Phosphorimetry, Theory, Instrumentation and Applications, VCH Publications, 1990.
[19] A.V. Deshpande, E.B. Namdas, J. Photochem. Photobiol. A 110 (1997) 177.
[20] G.R. Fleming, A.W.E. Knight, J.M. Morrison, R.J. S Morrison, G.W. Robinson, J. Am. Chem. Soc. 99 (1977) 4306.
[21] M. Megata, T. Kubota, Molecular Interaction and Electronic Spectra, Ch. 8, Marcel Dekker, New York, 1970.
[22] J.B. Birks, Photophysics of Aromatic molecules, vol. 1, Ch. 8, Wiley Interscience, New York, 1970.
[23] C.A. Parker, C.G. Hatchard, Trans. Faraday Soc. 57 (1961) 1894.
[24] B.P. Straughn, S. Walker, Spectroscopy, vol. 3, Chapman and Hall, 1976, pp. 188–189.
[25] M. Casalboni, R. Senesi, P. Prosposito, F. De Matteis, R. Pizzoferrato, Appl. Phys. Lett. 70 (1997) 2969.
[26] K.S. Lam, D. Lo, K.H. Wong, Opt. Commun. 121 (1995) 121.
[27] L.L. Hench, J.K. West, Chem. Rev. 90 (1990) 33.
[28] A.V. Buettner, J. Phys. Chem. 68 (1964) 3253.